

PAPER • OPEN ACCESS

Predictable and robust performance of a Bi-2223 superconducting coil for compact isochronous cyclotrons





To cite this article: C H Vermeer *et al* 2023 *Supercond. Sci. Technol.* **36** 045018

View the [article online](#) for updates and enhancements.

You may also like

- [Quench and self-protecting behaviour of an intra-layer no-insulation \(LNI\) REBCO coil at 31.4 T](#)
Y Suetomi, T Yoshida, S Takahashi et al.
- [Review of recent developments in ultra-high field \(UHF\) NMR magnets in the Asia region](#)
Y Yanagisawa, M Hamada, K Hashi et al.
- [High temperature superconductors for commercial magnets](#)
Arno Godeke

Predictable and robust performance of a Bi-2223 superconducting coil for compact isochronous cyclotrons

C H Vermeer^{1,2,*} , A H Tolboom², S J Otten² , H J G Krooshoop², R Lubkemann¹, J Leferink², W A J Wessel², A Nijhuis^{1,2} , A Godeke³ , M Walpole⁴, J Heese⁴, K Hayashi^{5,6} and E Shizuya⁵

¹ Foundation SuperACT, Marterstraat 66, 7559 AJ Hengelo, The Netherlands

² University of Twente, PO Box 217, 7500 AE Enschede, The Netherlands

³ Independent Consultant, Hengelo, The Netherlands

⁴ Varian Medical Systems Particle Therapy GmbH & Co. KG, Mottmannstraße 2, 53842 Troisdorf, Germany

⁵ Sumitomo Electric Industries, Ltd, 1-1-3, Shimaya, Konohana-ku, Osaka 554-0024, Japan

⁶ Kyoto Future Medical Instruments Inc., 15, Shimogamo-morimoto-cho, Sakyo-Ku, Kyoto 606-0805, Japan

E-mail: c.h.vermeer@utwente.nl

Received 16 September 2022, revised 12 January 2023

Accepted for publication 8 February 2023

Published 7 March 2023



Abstract

The development of ever smaller medical particle accelerators is motivated by a desire to make proton therapy accessible to more patients. Reducing the footprint of particle accelerators and subsequently proton therapy facilities allows for cheaper and broader usage of proton therapy. By employing superconducting technologies for field shaping, the size of particle accelerators can be reduced further below what is possible with saturated iron. This article discusses experiments on a first-of-its-kind double pancake (DP), and an assembly of six DP coils, designed to be used as a so-called ‘flutter coil’ for a compact isochronous cyclotron for proton therapy, fabricated from high-temperature superconducting (HTS) $\text{Bi}_{2-x}\text{Pb}_x\text{Sr}_2\text{Ca}_2\text{Cu}_3\text{O}_y$ (Bi-2223) tape. The coils were mounted under pre-stress within a stainless-steel structure to maintain mechanical stability during the experiments. The critical current as a function of the temperature of both coils was measured in a conduction-cooled setup. A model describing the coils, based on tape data, was created and revealed that the measurements were in excellent agreement with the predictions. Additional experiments were performed to study the quench and thermal runaway behaviour of the HTS coils, determining whether such coils can be protected against fault scenarios, using realistic quench-detection levels and discharge extraction-rates. These experiments demonstrate that the coils are very robust and can be well protected against quenches and thermal-runaway events using common quench-protection measures with realistic parameters.

* Author to whom any correspondence should be addressed.



Original Content from this work may be used under the terms of the [Creative Commons Attribution 4.0 licence](https://creativecommons.org/licenses/by/4.0/). Any further distribution of this work must maintain attribution to the author(s) and the title of the work, journal citation and DOI.

Keywords: proton therapy, superconducting coil, Bi-2223, cyclotron

(Some figures may appear in colour only in the online journal)

1. Introduction

The large-scale implementation of proton therapy is hampered by its large footprint and the high initial investment, while many patients can benefit from the reduced irradiation of healthy tissue enabled by this technology. Proton therapy treatment facilities usually consist of an accelerator (cyclotron or synchrotron), an energy selection system, a beam transport system, and 2–5 treatment rooms equipped with a gantry and an additional 1 or 2 fixed beamlines. Depending on the layout and number of treatment rooms, such facilities typically have a footprint of 1000–3000 m². Although single-room facilities are emerging, consisting of a single cyclotron or a synchrotron coupled to a gantry, these facilities are still relatively large, with a footprint in the order of 400 m². These single-room proton facilities are less available than photon treatment facilities. More compact and affordable proton treatment facilities can be enabled by using superconducting technologies.

Several studies show that proton therapy can benefit from superconducting magnets in the beam guidance up, over, and into the patient (the gantry) [1–5]. Besides using superconducting magnets for gantries, proton accelerators (typically a cyclotron) can also benefit from superconducting magnets [6, 7]. A detailed design for such a compact isochronous cyclotron magnet and suitable conductor has been described by Godeke *et al* [8]. Bi_{2-x}Pb_xSr₂Ca₂Cu₃O_y (Bi-2223) high-temperature superconducting (HTS) tape has been selected as a suitable conductor for the flutter coil (FC). Sumitomo Electric Industries, Ltd (SEI) successfully demonstrated that they were able to wind a curved double pancake (DP) [9] from this tape and manufactured two coils: a DP and a FC assembly comprising six DP coils. The tapes are wound for each pancake along a stainless-steel 316L coil former. The FC consists of stacked DP's with copper cooling-plates and glass epoxy plates for electrical insulation. The FC kidney-shaped design has strongly concave windings.

In this article we, discuss measurements performed on the DP and the FC in a conduction-cooled test environment in relation to the tape data used for modelling the coil's anticipated performance. First, the critical-current measurements at various temperatures of both coils are described. In addition, the quench behaviour is presented as well as the comparison between the model and the measurements. Finally, the DP and the FC were intentionally driven to their intrinsic limits by subsequent quenching, providing ultimate insight into the protection of such a coil.

2. Tape data

The superconducting tape used for the fabrication of the coils is Sumitomo DI-BSCCO Type HTi-SS tape, laminated with stainless-steel 304 for reinforcement and insulated with a

double wrap of 5 μm polyimide tape. The total length of superconducting tape in the DP is 229 m and in the FC 1374 m. The coil inductance of the DP is about 18.5 mH at 1 Hz and for the FC about 440 mH at 1 Hz. The critical-current and, therefore, self-field is dominated by the field-component perpendicular to the tape as presented by Kitaguchi *et al* [10]. The $I_c - B - T$ relation for the field-component perpendicular to the Bi-2223 Type HTi-SS tape is presented in figure 1 [11] and the n -index is extracted from [10]. The relation between the electric-field criterion, n -index representing the steepness of the transition from superconducting to the resistive state, and the critical-current I_c is $E/E_c = (I/I_c)^n$.

3. Measurement setup

There is a need to support both coils (in particular the concave section) against Lorentz forces [8]. A stainless-steel clamping structure with Ti-6Al-4V wedges was designed and fabricated for applying and maintaining precompression during cool-down, see figure 2. To have the same amount of compression on the winding pack of the coils, a precompression on the titanium wedges of 15 MPa for the FC and 2.5 MPa for the DP was applied. Cover plates with Belleville washers were placed in the axial direction to support the windings, especially to compensate for the more significant axial contraction of the windings compared to the coil. The outer coil-perimeter is not a smooth surface, and to ensure that the coil was compressed uniformly, a filler was required between the coil and the stainless-steel clamping structure. This filler material must withstand cryogenic temperatures and match the thermal expansion coefficient of the surrounding steel and coil windings. LOCTITE® STYCAST® 2850 FT with catalyst 23LV was used as filler material, see figure 2. This layer was only required as filling material and must be removable to make sure the coil and the clamping structure do not become bonded and the clamping structure could be used for both coils. Therefore, three layers of release agent QZ 13 were applied to the contact perimeters. To create a uniform gap between the coil and stainless-steel clamping structure, and to split the epoxy layer and remove the layer after testing, glass epoxy breaker pins were added. The coil with the stainless-steel clamping structure was placed on a flat table with a silicone rubber sheet as shown in figure 2. Then the STYCAST® was injected with syringes having needles of 1.8 mm outer diameter. The epoxy was pumped before injection to approximately 500 Pa to ensure a gas-free mixture. After curing, an insulation resistance test was performed with a Gossen Metrawatt® METRISO PRIME revealing no contact to ground at 250 V for both coils.

The tests at the University of Twente were performed in a vacuum cryostat test-facility, with three Sumitomo Heavy Industries, Ltd CH-110 Gifford-McMahon coolers [12]. One

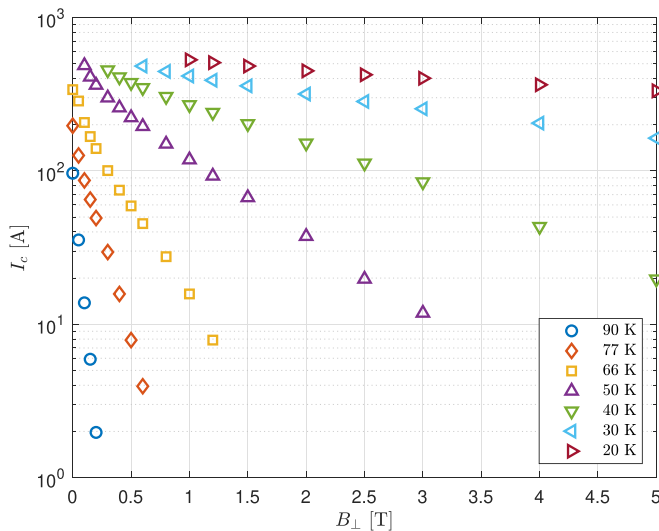


Figure 1. $I_c - B - T$ relation for field perpendicular to Bi-2223 Type HTi-SS tape [11].

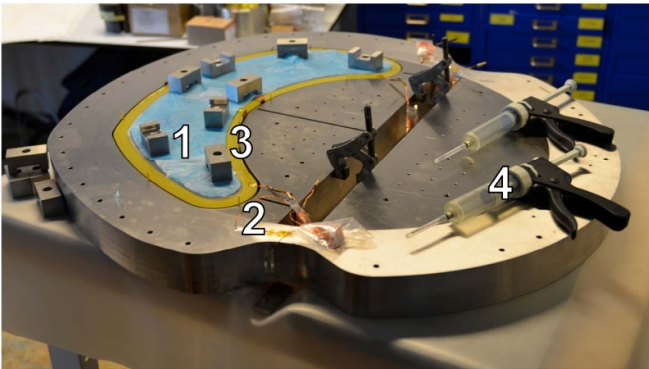


Figure 2. Flutter coil covered with foil (1) inside the clamping structure (2) before filling the gap (3) with STYCAST[®] using syringes (4). The flutter coil isolated from the clamping structure can be found in figure 9, clearly showing the kidney-shaped design.

cooler for the radiation shield and current leads, and two coolers for the coil and stainless-steel 304 clamping structure, using copper flex-links and busbars, as presented in figure 3. The copper busbars are made from electrolytic tough pitch (ETP) copper with an initial residual resistivity ratio (RRR) of 50 ($R_{273\text{K}}/R_{20\text{K}}$). Giving the ETP copper bars a heat-treatment at 632 K for 4 h increases the RRR to 110 ($R_{273\text{K}}/R_{20\text{K}}$). Eight Lakeshore Cernox temperature-sensors were placed directly onto the coil; four at the top and four at the bottom. In addition, temperature sensors and heaters were placed to control the surrounding stainless-steel structure's temperatures and enable the copper cooling-links to reach the desired temperature. For the current leads from the heat-sink connection at the cooler side to the coil terminations, $\text{ReBa}_2\text{Cu}_3\text{O}_{7-\delta}$ (ReBCO) tape was used. Two ReBCO tapes were placed in parallel with a combined critical-current capacity exceeding 1000 A at 20 K. The HTS tapes were mechanically supported by means of a copper strip with a thin epoxy layer for proper thermal contact and mechanical fixation. The connections between the current

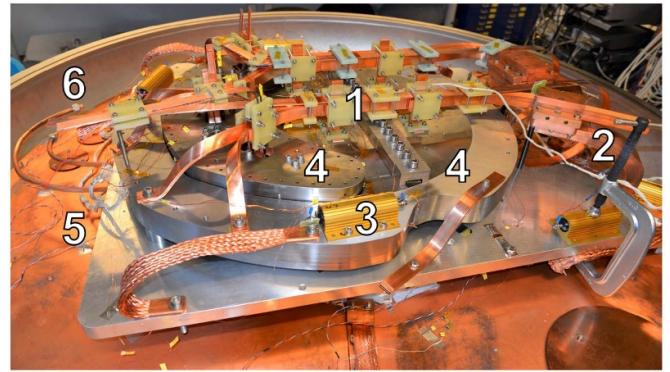


Figure 3. The entire assembly including coil, cooling-busbars (1), cooling-links (2), heaters (3) and clamping structure (4) in the measurement setup, consisting of a radiation shield (5) and vacuum chamber (6).

leads were electrically made by firmly pressing indium wire between the joints. The current leads were placed on top of the copper cooling-busbars with sapphire discs in between for a thermally conducting but electrically isolating connection.

Four strain-gauges were located on the narrow outer sections of the stainless-steel ring to measure the pre-compression. In addition, two reference strain-gauges were glued onto a small piece of stainless-steel that was not subjected to any applied load. These pieces were heat-sunk using Apiezon N grease to measure the resistance change of the strain-gauges due to the temperature change. The heaters on the stainless-steel clamping structure and the cooling-busbars were controlled to reach the desired equilibrium-temperatures. Although multiple voltage-taps were placed on the coils and current leads, all critical-current measurements were based on the voltage over the entire coil, excluding the current leads. The voltages were measured using Keithley[®] 2000 multi-meters. The measurements started at 84 K, at which the current and stored energy are relatively low. To study a quench, the voltage signals during the quench measurements were recorded by a Yokogawa[®] DL850E oscilloscope with 16 bit isolated modules and sampling rate of 1 MS s^{-1} .

4. DP measurement results

The single DP coil was charged with a current of 10 mA during cool-down to measure the critical temperature (T_c). Cool-down took approximately three days before reaching the final temperature of about 20 K. During cool-down, the temperature sensors on the coil stayed within $\pm 1 \text{ K}$. The normal to superconducting transition is 108 K, as can be derived from figure 4, in which the voltage is plotted as a function of the average temperature of the coil. The measured transition is in good agreement with the critical temperature found in the literature [13, 14].

4.1. Critical-current measurements

The tests include critical-current (I_c) measurements and quench testing. The I_c measurements were performed at 84 K,

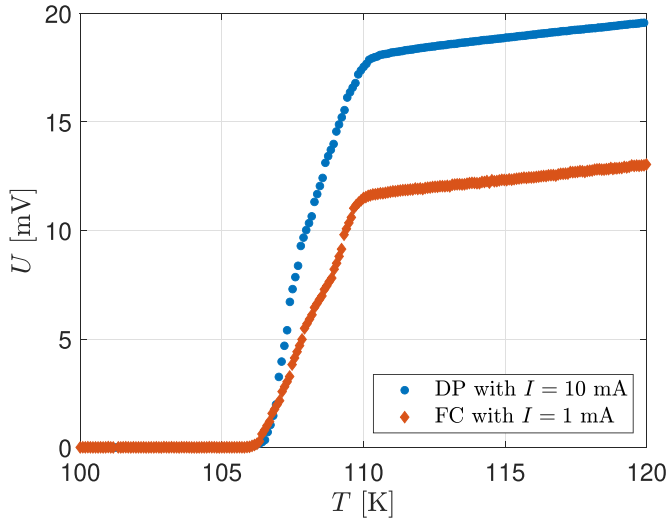


Figure 4. Total coil-voltages as a function of the average temperature of the temperature sensors of the double pancake and the flutter coil during cool-down.

77 K, 60 K, 45 K, 30 K and 20 K. At 77 K, the results are compared with the liquid nitrogen results from SEI. In figure 5, the voltages as a function of the currents for the critical-current measurements performed on the DP are presented, with U_0 representing the offset-voltage recorded before the individual measurements. The coil current was increased until $U - U_0$ was approximately 10 mV. The threshold-value of $E_c = 10 \mu\text{V}\cdot\text{m}^{-1}$ ($U - U_0 = 2.29 \text{ mV}$) along the entire tape length of the coil is used for the I_c calculations [15]. The resulting critical-currents at the various temperatures are presented in table 1. As this is a conduction-cooled measurement setup, the coolers used have limited cooling-power at lower temperatures. Since the heat-capacity of the DP is relatively small, the temperatures during the I_c measurements at the lowest temperature are slightly increasing, reducing the critical-currents. Increasing the temperature during an I_c measurement will also increase the slope since the transition to the normal state is reached earlier, thereby, lifting the n -indexes [16].

During cool-down of the DP, the strain-gauges were monitored and compared to the reference strain-gauges. Since the clamping structure is designed for the FC, the system is over-dimensioned for the DP. Because the temperatures at the locations of the strain-gauges differ during cool-down, especially for the reference strain-gauges compared to the strain-gauges on the stainless-steel, strain-monitoring during cool-down was not very accurate. Once a stable situation was reached and all measured temperatures were controlled to roughly the same temperature, the differences between strain-gauges could be more accurately evaluated. The clamping structure was designed to maintain the precompression on the winding pack, applied at room-temperature, during cool-down [8]. However, the applied precompression of 2.5 MPa on the DP from room temperature to 84 K down to 30 K doubled. At 20 K, a significant difference in resistance of the strain-gauges on the stainless-steel ring was observed compared to

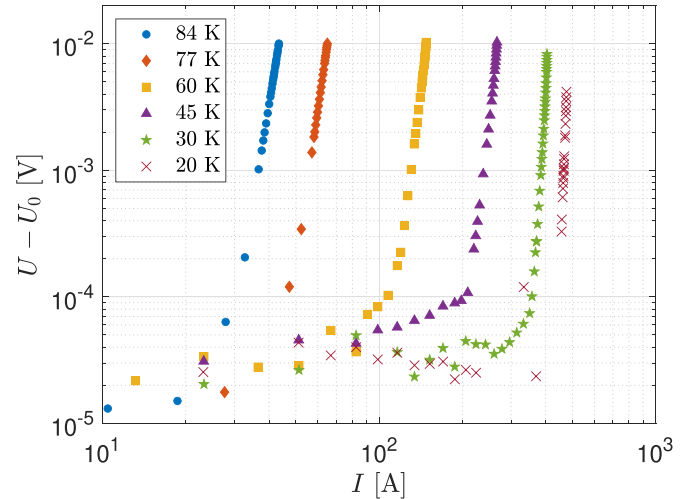


Figure 5. VI -curves of critical-current measurements at various temperatures for the double pancake.

Table 1. Results of the critical-current measurements for the double pancake at $E_c = 10 \mu\text{V}\cdot\text{m}^{-1}$. The n -indexes at 30 K and 20 K are in italic since these values likely increased due to the small temperature increase during the measurements.

T (K)	I_c (A)	n -index (-)	$T_{\text{increase at } I_c}$ (K)
84	39	13.6	0.05
77	59	15.3	0.08
60	137	17.7	0.35
45	249	18.1	0.72
30	396	<i>30.7</i>	1.65
20	471	<i>62.1</i>	1.97

the reference strain-gauges, suggesting the precompression returning to its initial value.

4.2. Quench measurements

Minimum quench energy (MQE) measurements were performed using a Minco[®] spot-heater, with a resistance of 10Ω , which was directly mounted on the outer surface of both windings of the DP. Activation of this heater simulates the case of a local weak section with reduced I_c . The MQE measurements were performed at 80% of I_c . At 77 K, with low energy stored in the coil, making it less likely to damage the coil from a quench, we started the MQE measurements, followed by MQE measurements at 30 K. Although faster extraction of the current is possible, a relatively long time constant (τ) of 20 s and a quench detection level of 10 mV were selected for the MQE experiments to stay close to conservative full FC system operational conditions [17]. A heater-pulse was given to the quench heater, starting with a short duration of the pulse (on the order of seconds) and low power (several watts). The time and energy of the pulse were gradually increased with an interval of ten minutes to make sure all temperatures were stabilised before giving a new pulse. Finally, a quench was triggered at a heater-pulse of 10 s with 5 W power

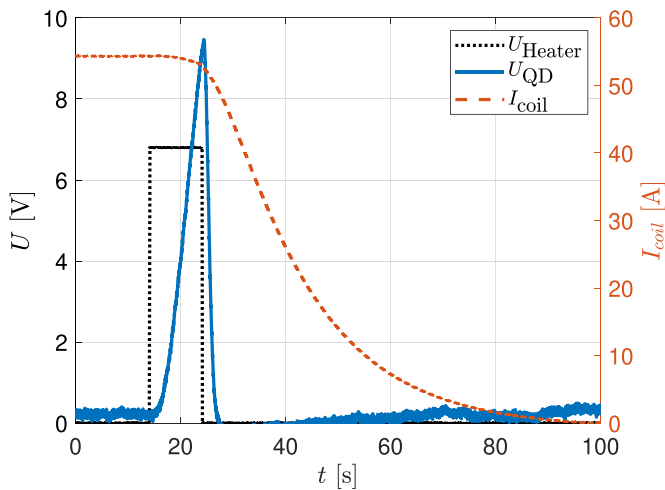


Figure 6. Quench detection trip-recorder signals using a Yokogawa DL850E oscilloscope (UQD amplified 1000 \times) at 77 K with a heater-pulse duration of 10 s and a current extraction time-constant of 20 s.

(50 J). The resulting quench detector (QD) signal (amplified by 1000 \times) and current decay, including heater-pulse, are presented in figure 6. The voltage-difference between the two halves of the DP coil (QD signal) increases due to a normal-zone formation. After reaching about 10 mV, at 23 s, the QD was triggered, draining the current in 20 s while a sharp decrease in the voltage of the entire coil was visible. After the MQE experiments, a critical-current measurement at 77 K revealed the coil remained undamaged since the critical current was not changed.

At 30 K and 80% of I_c , the DP could not be quenched using the maximum power of the Minco heaters of 5 W, even when applying 150 J (5 W for 30 s). Since one of the aims of the coil test was exploring its intrinsic limits, the test conditions were further stepped up. Finally, after setting the current to 88% of I_c , the DP quenched at 80 J heater energy. Once the quench was initiated, the current started to decay with a τ of 20 s. But only 2 s into the current decay, a sharp decrease occurred, followed by a loud sound, clearly audible outside the cryostat. At 30 K, more energy is present in the coil, making the quench more violent. After the quench, an I_c measurement was performed, revealing a resistive part that could entirely be credited to the bottom half of the coil as the top half remained superconducting. Although the quench-heater remained intact, the coil resistance to ground decreased from several M Ω to 1.2 k Ω measured using a Keithley[®] 2000 multimeter.

Dismantling the DP revealed a clear sign of a local hot-spot at the bottom half of the DP. In addition, burned Apiezon was found on the Aluminium bottom support-plate and a burned oxide-layer on top of the base support-structure. The colour of the oxide layer indicates that locally very high temperatures were reached (around 600 K) as these colours are observed in metallurgy when tempering stainless-steel. Figure 7 shows the local hot-spot on the coil and the material deposited on the base support-structure.

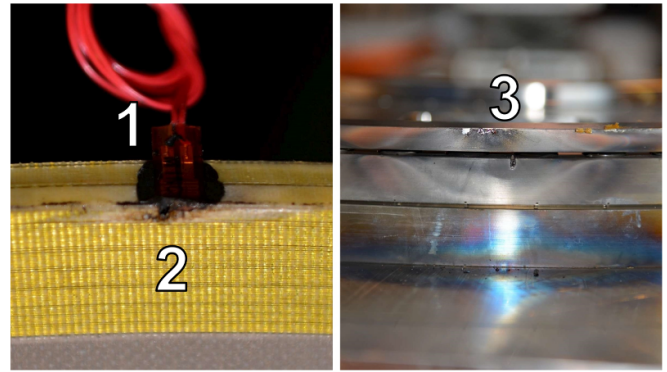


Figure 7. Visual inspection after the MQE intrinsic limit test at the location of the quench heater (1), revealing a local hot-spot at the DP (2) and base support-plates (3).

5. FC measurement results

During cool-down the FC was charged with 1 mA to measure the critical temperature. The resulting voltage is presented in figure 4. The superconducting transition is 108 K [13, 14].

5.1. Critical-current measurements

The voltages as a function of the currents for the critical-current measurements are presented in figure 8. The critical-currents, n -indexes, and temperature increases during the measurement are listed in table 2. For the FC the critical-current criterion is equal to that of the DP, namely $E_c = 10 \mu\text{V}\cdot\text{m}^{-1}$ ($U - U_0 = 13.74 \text{ mV}$). SEI tested the FC in a liquid nitrogen bath without applying any pre-tension, resulting in a critical current of 38 A at the criterion of $E_c = 10 \mu\text{V}\cdot\text{m}^{-1}$. Also for the FC, a small temperature increase is observed at I_c , albeit less than at the DP suggesting a reduced impact on the n -index due to the larger heat-capacity of the FC.

The strain-gauge data revealed no significant change in applied precompression of 15 Mpa at various temperatures, except for 20 K, where a slight reduction of about 20% in precompression was observed.

5.2. Quench measurements

Although the MQE experiments performed on the DP are instructive, the experiments only simulate what will happen in the case of a local low I_c in the conductor. The quench heaters are not positioned in the peak-field region of the coil, and even then, it can be debatable whether activating the quench-heater is simulating a quench, such as can be expected in a final cyclotron setup, or still only simulates a local limitation of I_c of the tape. A quench-heater only heats a small volume-fraction of the winding pack. At the same time, the tape remains superconducting closely around the local hot-spot since the normal-zone propagation velocity is low, because of the large heat-capacity and the high critical-temperature (T_c). A low propagation speed of the normal-zone remains challenging to detect. It is anticipated that for a cyclotron magnet-system, a

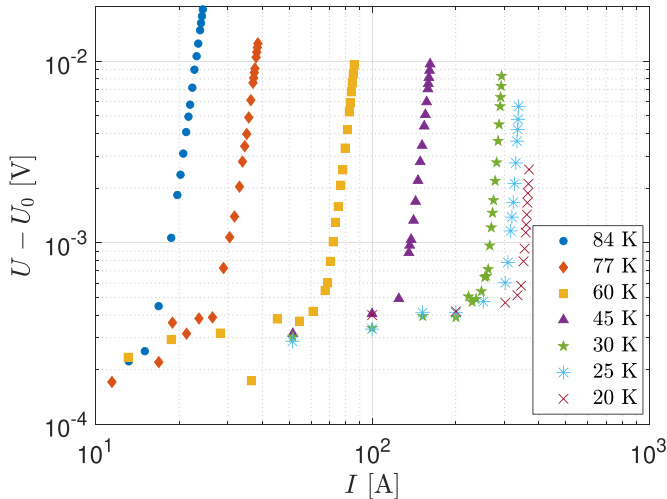


Figure 8. VI -curves of critical-current measurements at various temperatures for the flutter coil.

Table 2. Results of the critical-current measurements on the flutter coil at $E_c = 10 \mu\text{V}\cdot\text{m}^{-1}$.

T (K)	I_c (A)	n -index (-)	$T_{\text{increase at } t_c}$ (K)
84	24	11.0	0.07
77	39	11.8	0.11
60	88	13.5	0.11
45	167	13.5	0.30
30	305	19.2	0.75
25	361	18.7	0.75
20	399	22.9	0.80

local weak-spot can be detected by I_c testing of the tape in advance in conductor quality-control. Therefore, simulation of a local weak-spot is less attractive in the FC test. The chosen alternative method is a transition to the normal state in large part of the conductor/coil by slowly increasing the current until a large conductor volume in the highest magnetic-field area surpasses I_c and starts developing sufficient voltage for detection. Protecting against too much (induced) current in the coil due to an operational mistake is a realistic worst-case scenario. In the test, this was simulated by increasing the current stepwise until thermal runaway occurred at static current and the quench detection system was triggered.

Crucial for this quench testing is whether a quench can be detected fast enough with sufficient resolution, and once detected, if the energy can be extracted fast enough to keep the coil safe. In the final cyclotron system design, a total of eight FCs are foreseen, and therefore an appropriate extraction time of 3 s is expected. Furthermore, a QD threshold-level of 20 mV is seen as a feasible quench detection level in the final application.

The chosen method requires a low QD voltage-threshold and a fast extraction time (τ) at the start. Consequently, the quench detection voltage-level and/or the extraction time were intentionally gradually increased to find the intrinsic limit of coil operation, which means reaching irreversible degradation of the coil. The quench detection voltage-level could easily be

Table 3. Quench testing of the flutter coil at 20 K and 385 A (96% of I_c .) in order as tested.

τ (s)	U_{QD} (mV)	Coil status (-)
0.7	5	OK
1.4	5	OK
1.4	10	OK
1.4	20	OK
2.2	20	OK
3.1	20	OK
3.8	20	OK
5.0	20	OK
6.0	20	OK
7.3	20	OK
3.1	40	OK
3.1	80	Not OK

adjusted on the QD, and the extraction time was adjusted by changing the resistance of the dump resistor. A faster extraction time consequently means a higher voltage-peak across the coil, and for operational purposes, the voltage-peak was constrained to 250 V.

The quench measurements are performed at 20 K and are listed in table 3. The FC was intentionally driven to its intrinsic limits in order to test the feasibility margin of detecting a quench and determining the extraction limits. Thermal runaway in this conduction-cooled coil, with cooling configurations as described in the measurement setup, starts to occur when approaching I_c due to the voltages and resulting losses that are generated in the coil in the transition close to the critical-current criterion. After reaching a static current of 96% of I_c (385 A) at which the temperatures and voltages slowly started to increase, it took approximately ten minutes before the QD was triggered, which allows more than sufficient time to protect the coil from quenching. After each quench test, the coil performance was evaluated by applying a small current and measuring the voltage to examine any possible degradation. The results clearly show that the coil can safely survive an extraction time of 7.3 s at a quench detection level of 20 mV. After increasing the QD threshold to an unrealistically high level of 80 mV, at 3.1 s of extraction time, the measurement after the quench test revealed a linear resistive component in the VI -curve. This resistive component only occurred in the bottom DP voltage-tap. All other sections remained superconducting.

After all experiments were performed, the system was warmed up, and the setup was disassembled for a visual inspection. This inspection revealed that at the bottom section, material (most probably tin and silver) locally burst out and deposited onto the copper cooling-plate, shown in figure 9.

6. Tape data versus coil performance

The tape $I_c(B, T)$ and n -index data were implemented in a COMSOL Multiphysics® model in which the coils were modelled as a lumped volume. The perpendicular magnetic field profile in the FC in the top DP, and due to the symmetry in

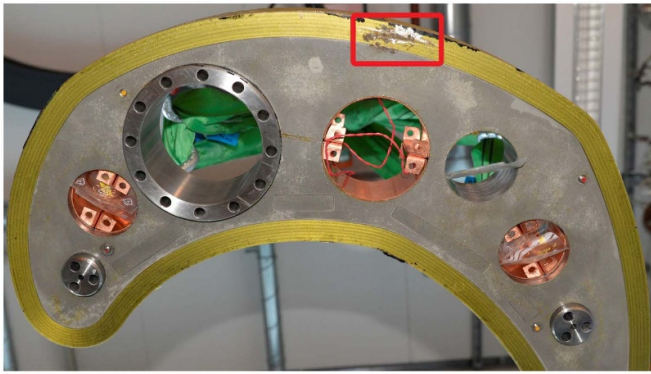


Figure 9. Visual inspection at the bottom of the flutter coil after intentionally driving the FC into over-current. The deposited material is highlighted in the red square.

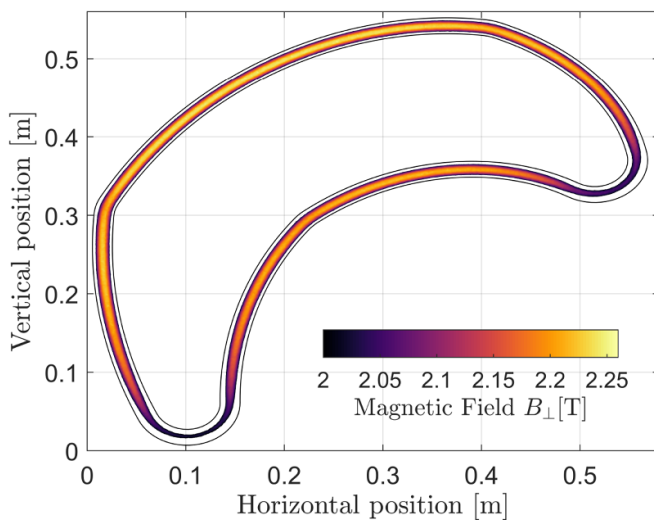


Figure 10. COMSOL Multiphysics® model of the radial field (perpendicular to the tapes) at 30 K and 290 A at the top of the Flutter coil.

the transverse plane also the bottom DP, at 30 K and 290 A is presented in figure 10. Although the axial field profile is highest in the sharpest corners of the ‘kidney’ shaped coil, the radial field is highest at a horizontal position of about 0.2 m and at a vertical position of about 0.5 m. The deposited material, indicating the damaged location found on the FC during the visual inspection, coincides with the location of the highest radial field, i.e. where the highest field is present perpendicular to the tape conductor.

The critical-current is extracted from the model by integrating the voltage at a given current, entirely determined by the field perpendicular to the tapes. The critical-current and n -indexes modelled this way and measured are presented in figure 11. Comparing the measurements with the model reveals that the FC is performing as expected with respect to the tape data. A similar model was made to describe the single DP with similar results compared to the measurement, with higher values in the measured n -index at the lower

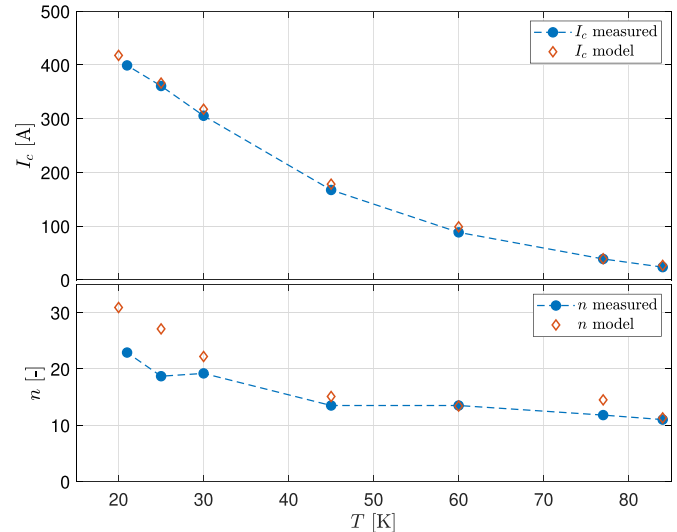


Figure 11. The critical currents and n -indexes as calculated using the model compared with the measured critical-currents and n -indexes of the flutter coil.

temperatures due to the smaller heat-capacity, as explained in the critical-current measurements of the DP. Although the model only considers the field contribution perpendicular to the tapes, the excellent agreement with the measurements shows that the axial field contribution in the coil plays a minor role. Assuming a dominating perpendicular field contribution to the tape is valid.

7. Discussion

The precompression is not expected to reduce at 20 K compared to 30 K since the linear contraction rate stagnates below approximately 40 K for the used materials. A possible explanation for the observed difference in strain-resistance is that the reference strain-gauges are not adequately cooled to 20 K since the reference strain-gauges are mounted on separate stainless-steel 304 blocks. These blocks are mechanically poorly fixed to the rest of the setup because the reference strain-gauges should only experience a change in temperatures but not any precompression created by the wedges. The thermal contact is made using Apiezon N grease. At 20 K, however, this thermal contact might be inadequate when practically no heater-power remains, and all cooling-power is utilised to cool the entire assembly. Therefore, the difference in pre-load between the higher temperatures and 20 K is explained not as an actual stress alteration but generated by the temperature difference between the reference strain-gauges and the strain-gauges on the outer ring due to the temperature dependency of strain-gauges.

Although mechanical stress can degrade the performance of the Bi-2223 tape, the mechanical pre-stress does not seem to decrease the performance as the model of the field perpendicular to the tapes describes the coils adequately. This

is consistent with transverse pressure measurements on the tapes, in which a 200 MPa limit was found [18].

8. Conclusions

The critical-current and n -index of two Bi-2223 coils for compact isochronous cyclotrons were successfully measured at various temperatures. A model describing the coil based on tape data revealed that the coil measurements are in excellent agreement with the model, meaning the performance of the coils can be well understood and predicted.

The quench testing on the DP with a heater to simulate local heating or a local weak-spot in the conductor, demonstrates the dangers if insufficient quality control is not performed by the conductor manufacturer, and a local low I_c is present in the conductor from which the coils are wound. It should be emphasized that sufficient quality control is clearly performed on the Bi-2223 conductor used in these coils. The quench tests on the FC, done by slow thermal runaway when approaching closely to I_c in a large coil-volume, show that sufficient voltage is developed for detection, with a convenient time period of approximately ten minutes before the quench detector is triggered. This demonstrates robust behaviour and sufficient scope for safe quench protection.

The quench tests reveal that a Bi-2223 FC is difficult to damage and can safely be protected against a quench or thermal runaway by using a solid-state relay, a voltage-threshold detection level up to 40 mV and a current extraction time constant of up to 7.3 s. Therefore, the Bi-2223 FC can be seen as a major step towards miniaturization of isochronous cyclotrons for proton therapy, opening the way to high-quality treatment rooms at a significant cost- and footprint-reduction.

Data availability statement

The data that support the findings of this study are available upon reasonable request from the authors.

Acknowledgment

The authors like to thank Sumitomo Heavy Industries (SHI) for their technical support and borrowing a cooler-compressor.

ORCID iDs

C H Vermeer  <https://orcid.org/0000-0001-9213-3916>

S J Otten  <https://orcid.org/0000-0002-1369-6903>

A Nijhuis  <https://orcid.org/0000-0002-1600-9451>

A Godeke  <https://orcid.org/0000-0002-8924-9878>

References

- [1] Felcini E, Bottura L, van Nugteren J, de Rijk G, Kirby G and Dutoit B 2020 *IEEE Trans. Appl. Supercond.* **30** 4400405
- [2] Nesteruk K P, Calzalaio C, Meer D, Rizzoglio V, Seidel M and Schippers J M 2019 *Phys. Med. Biol.* **64** 175007
- [3] Brouwer L, Caspi S, Hafalia R, Hodgkinson A, Prestemon S, Robin D and Wan W 2017 *IEEE Trans. Appl. Supercond.* **27** 4400106
- [4] Sanfilippo S, Calzalaio C, Anghel A, Gerbershagen A and Schippers J M 2016 Conceptual design of superconducting combined-function magnets for the next generation of beam cancer therapy gantry *Proc. RuPAC2016 (St. Petersburg, Russia)* p THCDMH01
- [5] Gerbershagen A, Calzalaio C, Meer D, Sanfilippo S and Schippers J M 2016 *Supercond. Sci. Technol.* **29** 083001
- [6] Schippers J M 2016 *Int. J. Radiat. Oncol. Biol. Phys.* **95** 149–53
- [7] Mohan R and Grosshans D 2017 *Adv. Drug Deliv. Rev.* **109** 26–44
- [8] Godeke A *et al* 2020 *Supercond. Sci. Technol.* **33** 064001
- [9] Hatanaka K, Fukuda M, Izumi N, Saito T, Ueda H, Yorita T, Yasuda Y, Kamakura K and Hamatani N 2012 Developments of HTS magnets *Proc. IPAC2012 (New Orleans, LA, USA)* p TUOAC02
- [10] Kitaguchi H, Takahashi K, Kumakura H, Hayashi T, Fujino K, Ayai N and Sato K 2009 *Supercond. Sci. Technol.* **22** 045005
- [11] Sumitomo Electric Brochure, Bi-2223 Superconducting Wire 2022 (available at: <https://sumitomoelectric.com/super/wire/wire-detail>)
- [12] Bergen A *et al* 2019 *Supercond. Sci. Technol.* **32** 125006
- [13] Polasek A *et al* 2005 *Mater. Res.* **8** 391–4
- [14] Shalaby M S, Hashem H M, Hammad T R, Wahab L A, Marzouk K H and Soltan S 2016 *J. Radiat. Res. Appl. Sci.* **9** 345–51
- [15] Pitel J 2013 *Supercond. Sci. Technol.* **26** 125002
- [16] Bergen A 2020 Conduction-cooled ReBCO coils for the wind converter: from laboratory to field test *PhD Thesis* University of Twente (<https://doi.org/10.3990/1.9789464190830>)
- [17] Yamaguchi T, Ueno E, Kato T and Hayashi K 2015 *Phys. Proc.* **65** 225–8
- [18] Pellen B 2021 Experimental and modelling studies of transverse load on DI-BSCCO tapes (University of Twente) (available at: <https://purl.utwente.nl/essays/94527>)